Research Square

Preprints are preliminary reports that have not undergone peer review.
They should not be considered conclusive, used to inform clinical practice,
or referenced by the media as validated information.

A Mixed Community of Skin Microbiome Representatives Influences Cutaneous Processes more than Individual Members

Kristin H Loomis
Johns Hopkins University Applied Physics Laboratory
Susan K Wu
Johns Hopkins University Applied Physics Laboratory
Amanda Ernlund
Johns Hopkins University Applied Physics Laboratory
Kristina Zudock
Johns Hopkins University Applied Physics Laboratory
Allison Reno
Clemson University
Kianna Blount
Johns Hopkins University Applied Physics Laboratory
David Karl Karig (dkarig@clemson.edu)
Clemson University https://orcid.org/0000-0002-9508-6411

Research

Keywords: Skin microbiome, skin proliferation, host-microbiome interaction, RNA sequencing, cutaneous transcriptome, human microbiome, human skin equivalents

Posted Date: February 24th, 2020

DOI: https://doi.org/10.21203/rs.2.24334/v1

License: This work is licensed under a Creative Commons Attribution 4.0 International License.
Read Full License

Version of Record: A version of this preprint was published on January 22nd, 2021. See the published version at https://doi.org/10.1186/s40168-020-00963-1.

Abstract

Background Skin, the largest organ of the human body by weight, hosts a diversity of microorganisms that can influence health. The microbial residents of the skin are now appreciated for their roles in host immune interactions, wound healing, colonization resistance, and various skin disorders. Still, much remains to be discovered in terms of the host pathways influenced by skin microorganisms, as well as the higher-level skin properties impacted through these microbe-host interactions. Towards this direction, recent efforts using mouse models pointed to pronounced changes in the transcriptional profiles of the skin in response to the presence of a microbial community. However, there is a need to quantify the roles of microorganisms at both the individual and community-level in healthy human skin. In this study, we utilize human skin equivalents to study the effects of individual taxa and a microbial community in a precisely controlled context. Through transcriptomics analysis, we identify key genes and pathways influenced by skin microbes, and we also characterize higher-level impacts on skin processes and properties through histological analyses. Results The presence of a microbiome on a 3D skin tissue model led to significantly altered patterns of gene expression, influencing genes involved in the regulation of apoptosis, proliferation, and the extracellular matrix (among others). Moreover, microbiome treatment influenced the thickness of the epidermal layer, reduced the number of actively proliferating cells, and increased filaggrin expression. Many of these findings were evident upon treatment with the mixed community, but either not detected or less pronounced in treatments by single microorganisms, underscoring the impact that a diverse skin microbiome has on the host. Conclusions This work contributes to the understanding of how microbiome constituents individually and collectively influence human skin processes and properties. The results show that, while it is important to understand the effect of individual microbes on the host, a full community of microbes has unique and pronounced effects on the skin. Thus, in its impacts on the host, the skin microbiome is more than the sum of its parts.

Background

Human skin provides a physical barrier between the body and the outside world, preventing the entry of irritants and pathogens, informing the development of immune responses, and regulating water loss [1–4]. Populations of microorganisms—the skin microbiome—reside on and within human skin. Different skin sites and individuals harbor varying compositions of microorganisms [5,6] with estimated densities ranging from 10^4 to 10^6 microorganisms per square cm [6].

The skin microbiome plays a role in directing cutaneous processes critical to human health and disease [7–11]. Many previous research efforts have detailed specific mechanisms of communication between commensal skin microorganisms and host tissue. For example, Staphylococcus epidermidis and Staphylococcus aureus have been found to induce distinct signaling pathways, leading to specialized modulation of the innate immune system [12]. Similarly, a cell wall component common to the Corynebacterium genus was found to modulate an additional pathway of the immune system [13]. In

disease states, abnormal microbiome compositions – often characterized by a reduced diversity of microorganisms – have also been linked to diabetes, psoriasis [14–16], and atopic dermatitis [17–21].

While a wealth of discoveries have been made regarding the impact of skin microbes on the host, the vast majority of efforts have focused on individual taxa, have concentrated on specific impacts on the skin, or have drawn conclusions statistically from human sampling studies. Much remains to be discovered in terms of the collective host pathways that skin microbes influence at the gene expression level, as well as the higher-level skin properties impacted through the modulation of these pathways.

Towards this end, germ-free mice (those reared without a microbiome) have offered a powerful tool. Analogous to studies in the gut, where the microbiome has been shown to modulate fundamental functions such as intestinal nutrient absorption and mucosal barrier fortification [22–24], studies in the skin have demonstrated microbiome modulation of wound healing [25] and epidermal differentiation [26]. Of particular relevance, Meisel et al. revealed that in healthy mice, the skin microbiome influences gene expression for a range of biological processes including the cutaneous immune response, cytokine production, epidermal differentiation, and epidermal development [26]. Despite these significant findings, additional efforts are needed to characterize the consummate influence of individual microbiome members on microbiome-host dialogue. In addition, the uniqueness of the human skin microbiome warrants the characterization of microbe-host interactions in human tissues [27,28].

Here, we examine how members of the human skin microbiota inform cutaneous processes when cultured both individually and in a mixed community. To accomplish this, we use microbial isolates from healthy human skin and three-dimensional human skin equivalents. The human skin equivalents, like germ-free mouse models, allow for carefully controlled studies of skin-microorganism interactions, [29] but they additionally support the study of human-specific tissues and microorganisms [30–33]. We study microbiome representatives from genera that commonly reside in the aerobic environments of the skin surface – Staphylococcus, Streptococcus, Bacillus, Roseomonas, Paenibacillus, Micrococcus, Corynebacterium, and Acinetobacter [5]. We investigate individual microorganism contributions to a collective community response by co-culturing individual microorganisms and mixed communities at the air-tissue interface.

Using transcriptomics and histological analyses, we find that the presence of a model microbiome led to significantly altered patterns of gene expression, influencing genes involved in the regulation of apoptosis, proliferation, and the extracellular matrix. Moreover, microbiome treatment influences the thickness of the epidermal layer, reduces the number of actively proliferating cells, and increases filaggrin expression. Many of these findings are evident upon treatment with the mixed community, but not detected in treatments by single microorganisms, underscoring the impact of a diverse microbiome on the skin-microbiome relationship. This work furthers our understanding of how microbiome constituents both individually and collectively influence skin processes and extends previous efforts in murine systems [26] to human tissue and relevant microorganisms.

Methods

Skin microbiome representatives. Bacteria used in this study were isolated from swabs of healthy human skin [34]. 16S ribosomal RNA sequences were obtained by Sanger sequencing (Genewiz, LLC). Forward and reverse reads were merged to form a consensus sequence, which was then classified using the SINA search and classify service against the small subunit references in the Greengenes, RDP, and SILVA databases [35]. The least common ancestor common across the classification databases was used to identify isolates. Table S1 shows the consensus 16S rRNA sequences and classifications.

Bacteria culturing. Bacteria were stored at -80 °C in in tryptic soy broth (TSB, Sigma Aldrich) supplemented with 10% glycerol. Bacteria were streaked on tryptic soy agar (TSA, Hardy Diagnostics) at room temperature until single colonies were visible. Individual colonies were then picked, inoculated into 3 ml of TSB, and cultured at 30 °C overnight. Overnight cultures were then diluted 1:500 and incubated for four hours to generate starter inoculation cultures. Corynebacterium sp. and Streptococcus sp., which grow more slowly than other bacteria used in this study, were cultured on TSA for up to four days, in the initial liquid culture for 72 hours, and then in the subsequent liquid culture for 18 hours.

OD and CFU/ml calibration curves. Starter inoculation cultures were used to generate seven cultures at dilutions ranging from 1:40 to $1:4 \times 10^6$ in TSB. Bacterial cultures were allowed to grow from four to 18 hours, and the optical density at 600 nm (OD) was measured using the cuvette reading mode on a Nanodrop 2000C spectrophotometer (Thermo Scientific). For cultures where the OD reading was between 0.1 and 1, bacteria were serially diluted from 1:100 to $1:10^6$ and plated in triplicate on TSA plates. The number of colony-forming units (CFU) was counted for each condition, and a linear regression was calculated using GraphPad Prism (version 8.1.1 for windows, GraphPad Software, La Jolla California USA, www.graphpad.com) to relate CFU/mL to the culture OD. These relationships are shown in Figure S2.

EpiDerm and bacteria co-culture. Underdeveloped full-thickness EpiDerm (EFT-400-7A, MatTek) was equilibrated and cultured in antibiotic-free culture media (MatTek) at 37 °C with 5% CO_2 and no humidification. Starter inoculation cultures were washed twice in phosphate buffered saline (PBS, Fisher BioReagents) by centrifugation at 8,000xG, removal of the supernatant, and then suspension of the cell pellet in fresh PBS. The cell concentration was then adjusted to 1×10^8 CFU/ml based on the established OD vs. CFU/ml relationships. For the mixed community treatment, equal volumes of cell suspensions were mixed to generate a total suspension of 1×10^8 CFU/ml. Once the EpiDerm tissues were fully developed, bacteria solutions were deposited at the air-tissue interface (see Fig. 1A) in two spots of 2.5 µl each. The axenic control condition was treated with the PBS vehicle only. For transcriptomics analysis, five tissues were used for each condition, and bacteria were incubated on the tissue for approximately 18 hours. For histological analysis, five to six tissues were used per condition, and bacteria were incubated on the tissues for five days.

RNA extraction and sequencing. To extract cellular RNA, tissues were immersed in Trizol and lysed by bead beating for five minutes at a 20 s^{-1} frequency using the Qiagen Tissue Lyzer with the Navy bead beating kit (Next Advance). Tissues homogenates were further lysed by passing through the Qiashredder (Qiagen). Homogenates were then extracted with chloroform, mixed with an equal volume of ethanol, and loaded into columns of an RNeasy mini kit (Qiagen), at which point the manufacturer's directions were followed, which included the on-column DNAse (Qiagen) digestion. RNA concentrations were determined using a Quant-it RNA Assay Kit with a Qubit 3.0 Fluorometer. Library preparation was performed using the QuantSeq 3' mRNA-Seq kit (Lexogen) and libraries were sequenced on a NextSeq using the 500/550 High Output v2 kit (Illumina) in 75 base pair single-read mode.

Sequence processing and analysis. Raw single-end FASTQ files were trimmed with Trimmomatic-0.35 and adapters were removed using default settings [36]. Both leading and trailing minimum quality scores were set to 20, a sliding window of 4:20 was used, and the minimum read length was set to 50. Transcript expression was quantified with Salmon [37] and transcript level abundance was summarized by gene-level analysis using the tximport package in R [38]. The human genome assembly hg38 (NCBI assembly ID 5800238) was used as the index and bootstrapping (with replacement) was set at 50. Differential abundance was calculated using DESeq2 [39] with a false discovery rate (FDR) threshold of 0.1 [40]. DESeq2 uses the Benjamin-Hochberg (BH) correction to calculate adjusted p-values. A Pearson correlation was performed to determine the similarity [41] of the five replicates for each condition (Table S3). The transcriptome coverage for each sample was also examined and are shown in Table S3. Replicates with Pearson correlations under 0.875 were removed, and the differential expression analysis was repeated for each condition. An adjusted p-value of 0.05 was used as a significance cutoff to determine differentially expressed genes. Euler diagrams were created with eulerAPE v3 [42].

Hierarchical clustering was performed using variance stabilizing transformed (VST) data for individual samples (as shown in Fig. 1B) [39] or log2 fold change (log2FC) values (as shown elsewhere throughout the paper) for aggregated treatment groups using average linkage in JMP® (Version 13.0.0, SAS Institute Inc., Cary, NC, 1989–2019) software. To examine expression levels of individual genes across tissues, VST-transformed data were plotted for individual tissues in a given condition.

Gene overrepresentation analysis. To gain insight on the biological processes influenced by microbiome treatment, genes that were differentially expressed between the mixed community treatment and axenic control were analyzed with Protein ANalysis THrough Evolutionary Relationships (PANTHER) analysis tools [43]. First, the number of genes differentially expressed between the mixed community treatment and the axenic control were functionally classified to the PANTHER GO-Slim ontologies of Molecular Function, Biological Function, and Cellular Component. The annotation was repeated using a list of genes that were differentially expressed in both the mixed community and single microorganism treatment. Next, the PANTHER classification system [43] was used to conduct an overrepresentation analysis (Released 2019-07-11) using the GO Biological Processes Complete annotation (version 14.1, released 2019-07-03) [44,44,45]. The input gene lists were based on all genes differentially expressed between the mixed

community and the axenic control with a BH-adjusted p-value < 0.05 (Table S4). Genes that were differentially expressed in the mixed community treatment condition but not in any single microorganism treatment were also examined using a BH-adjusted p-value of < 0.05. A background list (included in Table S5) consisted of all genes detected across all samples in the experiment with a base mean over 1. To determine statistically overrepresented gene sets, the Fisher's Exact Type test with a FDR correction was used. Reduce and Visualize Gene Ontology (REViGO)[41] was used to summarize the list of gene sets and finds representative subsets. For analyses of the mixed community, the list of gene sets with a FDR p-value < 0.01 were input into REViGO using the Homo sapiens database, the Resnik (normalized) similarity measure, and allowing for medium similarity. The resulting treemap was generated using p-values to determine box size and was visualized using JMP statistical software. The REViGO treemap for the gene sets enriched in the mixed community but not single-microorganism treatments, gene sets with an FDR p-value < 0.05 was used.

Histology and immunofluorescence staining. EpiDerm tissues were removed from transwell inserts using a sterile scalpel and immediately incubated in 4% paraformaldehyde diluted in PBS. The Johns Hopkins University Reference Histology Center then embedded tissues in paraffin and obtained 5-µm thick sections. Tissues were deparaffinized and rehydrated by treatment in xylene and ethanol and then stained with hematoxylin and eosin (H&E). For immunofluorescence analysis, after deparaffinization, slides were submerged in citric acid antigen retrieval solution (BD Biosciences) under steam treatment for 20 minutes. Tissues were allowed to cool at room temperature for 30 minutes, were washed three times in PBS for five minutes, and then permeabilized by incubating for 15 minutes in 0.1% triton-X 100 in PBS. Sections were then blocked by incubation in 5% bovine serum albumin (BSA) in PBS for 30 minutes at 37 °C, stained with a primary antibody overnight at 4 °C in a humidification chamber, washed three times in PBS for two minutes each, and then incubated with 1:200 dilutions of secondary antibody in PBS with 1% BSA. Unbound secondary antibody on the sections was washed away with PBS twice, and the tissues were then stained with DAPI for five minutes, and finally mounted with ProLong Gold (ThermoFisher Scientific). Primary antibodies were mouse anti-filaggrin (Santa Cruz Biotech # sc-66192), rabbit anti-loricrin (Biolegend, # 905104), and rabbit anti-KI67 (Novus, # NB500-170). Secondary antibodies were goat anti-rabbit Alexa fluor 594 (Thermo Fisher, R37117) and goat anti-mouse Alexa fluor 488 (Thermo Fisher, A-11001).

Tissue imaging and image analysis. H&E sections were imaged using a Motic EF-N Plan 10x objective with a 0.25 numerical aperture on a Motic BA210 microscope equipped with an EOS Rebel SLI camera controlled by Canon EOS software. Auto brightness and background adjustments were made to the images. Epidermal thickness was assessed in H and E sections by measuring the nucleated epidermal region of 10 or more randomly selected regions per tissue. The average thickness is plotted from 5 tissues per treatment condition. An ordinary one-way ANOVA followed by Dunnett's multiple comparisons test was used to compare differences from the axenic control.

Fluorescently stained tissues were imaged using a 10x objective on a Leica SPE confocal microscope controlled by Leica Application Suite X. The Leica Application Suite X was also used to generate a

mosaic image and maximum-intensity projections of z-stacks. Image J1.52 s was used to count the number of KI67^{+}, filaggrin positive, and loricrin + cells. In each case, maximum-intensity projections were smoothened and then binary images were generated based on a constant fluorescence intensity threshold. The 'analyze particles' tool was used to count the number of cells, limiting for circularity from 0.5-1 and a size cutoff of 30,000[46].

Results

Microbiome representatives alter skin tissue gene expression.

To examine the impact of individual microorganisms on the skin tissue processes, model microbiome treatments were co-cultured at the air-tissue interface of EpiDerm skin tissue equivalents (see Figure 1A). The inoculation density of each treatment condition was standardized to 5x10^{5} CFU per tissue. After 18 hours of co-culture, tissues were subjected to transcriptomic analysis. To examine the degree to which individual treatment conditions led to distinct changes in gene expression, we performed a hierarchical clustering analysis on data from biological replicates of each treatment condition (See Figure 1B). While the axenic treatment conditions are clustered together, many tissues treated with individual microorganisms are interspersed and are not organized into clear and discrete clusters, suggesting that individual microorganisms elicit some overlapping responses in the host skin tissue. However, tissues treated with the mixed community are clustered more closely suggesting that they elicit a more distinct response from the individual treatments. Indeed, the volcano plots in Figure 1C show that some microbiome treatments elicit more pronounced alterations in gene expression (e.g. *Micrococcus sp.*) than others (e.g. *Streptococcus sp.).* Interestingly, we also see that *Staphylococcus sp*. treatment appears to elicit a greater downregulation of genes compared to the other single-microorganism treatments. To visualize relationships between each biological treatment group, a heat map of altered gene expression for the entire transcriptome is shown in Figure 2A. Hierarchical clustering groups the *Streptococcus sp*. and *Roseomonas sp*. treatments, which led to the least pronounced responses. Notably, the mixed community treatment is distinct from the remaining single-microorganism treatments.

Microbiome representatives lead to distinct alterations in tissue gene expression.

To examine how similar tissue responses were to each microorganism treatment, we compared how many differentially expressed genes (those with an adjusted p-value <0.05) were shared across treatment groups (Figure 2B). Interestingly, we see that each treatment group elicits distinct changes in gene expression. For example, the *Staphylococcus sp.* and *Roseomonas sp.* treatments, which clustered closely in Figure 1B and 2A) both lead to the upregulation of 31 genes, but the downregulation of 117 and 10 genes, respectively. They only share two upregulated genes in common (RNY5 and CPT1A) and do not share a single downregulated gene. *Acinetobacter sp*. and *Corynebacterium sp.* treatments are also clustered together in the hierarchical analysis (Figure 2A), yet the differentially expressed genes elicited by each treatment have only partial overlap. *Corynebacterium sp.* and *Acinetobacter sp.* treatments led to the upregulation of 174 common genes, comprising 60% of those upregulated by *Acinetobacter sp.*

treatment and 40% by *Corynebacterium sp.* treatment. They elicited a common 24 downregulated genes, 41% of the 58 downregulated by *Acinetobacter sp*. treatment and approximately 9% of the 270 elicited by *Corynebacterium sp*. treatment. Indeed, each microorganism leads to distinctive responses from the host skin tissue.

We next examined how unique the response of each single-microorganism treatment response was to all other single-microorganism treatments. Additionally, we compared how much each single-microorganism treatment informed the response to the mixed community. Euler diagrams (shown in Figure 2C) visualize these comparisons. Compared to all other conditions, six of the eight single-microorganism treatments lead to the differential expression of unique genes. It is also interesting to see that a portion of genes up and down-regulated by the mixed community treatment are not altered in any single-microorganism treatment. The portion of genes unique to the mixed community treatment underlies the importance of studying individual taxa in the presence of their microbiome community.

Mixed community treatment leads to the overrepresentation of genes involved in a variety of biological processes. To understand the functional role of the differentially expressed genes, genes were classified into the high-level PANTHER GO-slim gene list (Figure 3A). A list of genes that were altered in the mixed community but not altered in any single microorganism treatment was also classified and shown in Figure 3A. Differentially regulated genes have primary molecular functions of binding and catalytic activity, and many of those genes were unique to the mixed community treatment. In biological process gene sets, many genes are involved in metabolic processes, cellular processes, and localization. Genes are active inside the cell, organelles, protein-containing complexes, and the extracellular region.

To more specifically examine the processes influenced by model microbiome treatments, we conducted a gene set overrepresentation analysis. A treemap showing gene sets that are significantly overrepresented by the mixed community treatment is shown in Figure 3B. A variety of biological processes were regulated, such as multicellular organism development, cell proliferation, regulation of apoptotic processes, and extracellular structure organization. To understand how the mixed community elicits unique responses to single-microorganism treatments, an additional gene overrepresentation analysis was conducted for genes differentially expressed in the mixed community treatment but not in any single-microorganism treatments (Figure 3C). Numerous gene sets were identified, and a majority (ten out of sixteen) were involved in metabolism.

Microbiome treatment influences epidermal thickness and cell proliferation in 3D skin tissue. One of the gene sets altered in our overrepresentation analysis was cell differentiation. To focus on genes involved in the differentiation and cornification of keratinocytes, we examined the expression of genes in the epidermal differentiation complex (see Figure 4A). Similar alterations in gene expression are observed across the treatment conditions. Qualitatively, the most prominent alterations are elicited in the mixed community treatment. Next, skin tissues co-cultured with microbiome treatments for five days were stained with H&E and examined with microscopy. The thickness of the nucleated epidermal region was measured and is plotted in Figure 4B. Tissues treated with either the mixed community or *Micrococcus*

sp. exhibit significantly reduced thickness. Representative images from each treatment condition are shown in Figure 4C. No other prominent alterations in tissue structure were observed.

Our gene set overrepresentation analysis also revealed alterations in cell proliferation. The expression of genes involved in the regulation of cell proliferation for all treatments is shown in Figure 5A. Again, we observe a similar pattern in gene expression across treatments; with a reduced effect observed in *Roseomonas sp*. and *Streptococcus sp*. treatments. Next, we examined the differential expression of the cell proliferation marker *MKI67* (Figure 5B). Mixed community treatment and four of the single-microorganism treatments (*Corynebacterium sp*., *Micrococcus sp*., *Paenibacillus sp*., and *Staphylococcus sp*.) lead to downregulation of *MKI67*. To expand upon these findings, we stained tissue sections for Ki-67 expression and counted the number of Ki-67^{+} cells. Again, tissues treated with the mixed community as well as *Corynebacterium sp*., and *Micrococcus sp*., had reduced numbers of proliferating cells (Figure 5C). Representative images are shown in Figure 5D. The proliferating cells are largely restricted to the basement of the epidermal region.

Microbiome treatment influences the expression of key epidermal proteins

Our examination of epidermal differentiation complex genes (Figure 4A), also showed that filaggrin and loricrin – two proteins important for skin barrier properties and skin structure – were impacted by microbiome treatment. Gene expressed of filaggrin and loricrin are shown in Figures 6A and 6B, respectively. Interestingly, only mixed community treatment leads to significant alterations in gene expression. However, a trend of loricrin upregulation is observed across many treatment conditions. To extend this finding to a functional alteration in skin tissue, we examined filaggrin and loricrin protein content in tissue sections. The number of cells staining positively for filaggrin content was quantified (Figure 6C). Only the mixed community treatment leads to an increased presence of filaggrin. We also examined the number of filaggrin cells and their intensity, but did not see significant alterations. Representative images are shown in Figure 6D. Changes in filaggrin and loricrin expression are observed qualitatively.

Discussion

Microbiome systems have been shown to interact with host tissues and regulate biological processes important in health and disease. In accord with previous skin microbiome studies in mice [26], we found that the microbiome regulates skin epidermal differentiation and homeostasis in human skin tissues. Beyond extending previous efforts to a human system, we examined how individual microbiome constituents inform cutaneous responses to a diverse model microbiome.

We showed that treatment of skin tissue with different single microorganisms elicited partly overlapping, but distinct responses in gene expression. We also revealed that host responses to the skin microbiome were not driven entirely by any single microorganism. The mixed community led to alterations in gene processes governing diverse biological processes including the immune response, epidermal

differentiation, cell proliferation, and metabolism. Moreover, we found that these changes in transcriptional profiles manifest in alterations to epidermal thickness, cell proliferation, and filaggrin protein content. Some of these effects were only observed in skin tissue treated with a mixed community of bacteria and not with single-microorganism treatments. For instance, treatment with Micrococcus led to decreased epidermal thickness, yet the greatest decrease in thickness was observed with the mixed community (Fig. 4). Several taxa reduce cell proliferation, but again, the most pronounced effect was associated with mixed community treatment (Fig. 5). Interestingly, significant increases in loricrin and filaggrin gene transcripts and filaggrin protein content were observed only for tissues treated with the mixed community, and not with any individual taxa. Collectively, these results suggest a strong community-effect of microbiome-host signaling, leading to changes in skin properties that are likely relevant to the heath and function of the skin.

It is important to note that the human skin equivalent model captures factors of the innate immune system, but not the adaptive immune system. While animal models may capture effects of a full immune system, we believe it is essential to investigate skin-microorganism interactions in human tissues, as humans have been shown to harbor skin microbiomes that are highly distinct, even from other primates [27,28]. Our skin model also lacks sebaceous glands and hair follicles, which prevents accurate biological simulation of Cutibacterium –a highly prevalent bacteria of the skin microbiome that primarily resides within the anaerobic environment of sebaceous glands. Future developments of more sophisticated tissue models may facilitate the accurate incorporation of Cutibacterium acnes.

Conclusions

Our efforts reveal important information regarding the effects of several prominent skin microbial taxa on human skin tissue and also point to a pronounced community-effect on the host skin that cannot be attributed to any single taxa acting alone. Again, this community-effect entails not only a distinct signature in the host transcriptional response profile, but also on epidermal thickness, cell proliferation, and observed filaggrin and loricrin. It is clear from this study and previous studies that individual microorganisms can elicit distinct responses from host tissue. However, we additionally find that host responses to individual bacteria are not fully predictive the responses to a mixed community. Thus, our results suggest that future studies aimed at examining microbiome constituents should consider the context of a microbiome community. In addition, we envision that this work, along with additional efforts to more specifically understand community-induced host-microbiome interactions, will inform therapeutic applications in the realms of synthetic biology and microbiome engineering.

Declarations

Ethics approval and consent to participate

Not applicable

Consent for publication

Not applicable

Availability of data and materials

Raw transcriptomic data files analyzed in this study are available in the Sequence Read Archive at https://www.ncbi.nlm.nih.gov/sra/PRJNA606973 or by searching for reference PRJNA606973.

Competing Interests

The authors declare no competing interests.

Funding

This material is based upon work supported by the U.S. Army Research Laboratory and the U.S. Army Research Office under contract/grant number #W911NF-14-1-0490.

Author Contributions

KHL and DK conceived the study design and wrote the manuscript. KHL and SKW performed the experiments. KB, TZ, and AE conducted sequencing and analysis. AR imaged and analyzed tissue sections.

Acknowledgements

We acknowledge Collin Timm for providing bacteria isolates, the Johns Hopkins core facility for providing histology services, and the Clemson Light Imaging Facility for using fluorescence imaging equipment. We also thank Julia Hannam and Delaney Di Gangi for microscopy.

Additional Files

Additional File 1 (.xlsx) Microorganism Isolate Information. Table containing information for the bacterial microorganisms used in this study. Table containing the identifying genus, the isolate identifier used by the collecting study, the 16S rRNA sequence, and the least common ancestors of the bacterial isolate determined by classification to the Greengenes, RDP, and SILVA databases. [34]

Additional File 2 (.pdf) Optical Density and Colony Forming Unit Standardization

Plots showing relationships between the colony forming units per milliliter and optical density at 600 nm of cultures for each bacterial isolate.

Additional File 3 (.xlsx) Quality Assessment of RNA-Sequencing Data

This file shows quality control metrics for the sequences of each individual sample. This includes the number of reads in the sample, the number and percentage of those reads that were mapped to the transcriptome, the number and percentage of total transcripts covered, and the number and percentage of total genes hit. Additionally, we assessed Pearson correlations of each individual sample within a biological treatment group.

Additional File 4 (.xlsx) Differential Gene Expression Data

This file contains the differential gene expression analysis for each microbiome treatment relative to the axenic control. Each gene included in the analysis is shown, including the basemean, log2 fold change, log2 fold change unshrunk, p-value, and adjusted p-value, as given by DESeq2.

Additional File 5 (.xlsx) Gene Set Overrepresentation Test Data

This file contains input and output information important to the Gene Set Overrepresentation Test. Genes used for the background gene list. The output data from the PANTHER Overrepresentation tests is also shown.

References

(1) Segre, J. A. Epidermal Barrier Formation and Recovery in Skin Disorders. *J. Clin. Invest.* **2006**, *116* (5), 1150–1158. https://doi.org/10.1172/JCI28521.

(2) Di Meglio, P.; Perera, G. K.; Nestle, F. O. The Multitasking Organ: Recent Insights into Skin Immune Function. *Immunity* **2011**, *35* (6), 857–869. https://doi.org/10.1016/j.immuni.2011.12.003.

(3) Proksch, E.; Brandner, J. M.; Jensen, J.-M. The Skin: An Indispensable Barrier. *Exp. Dermatol.* **2008**, *17* (12), 1063–1072. https://doi.org/10.1111/j.1600-0625.2008.00786.x.

(4) Grice, E. A.; Segre, J. A. The Skin Microbiome. *Nat. Rev. Microbiol.* **2011**, *9* (4), 244–253. https://doi.org/10.1038/nrmicro2537.

(5) Grice, E. A.; Kong, H. H.; Conlan, S.; Deming, C. B.; Davis, J.; Young, A. C.; NISC Comparative Sequencing Program; Bouffard, G. G.; Blakesley, R. W.; Murray, P. R.; et al. Topographical and Temporal Diversity of the Human Skin Microbiome. *Science* **2009**, *324* (5931), 1190–1192. https://doi.org/10.1126/science.1171700.

(6) Grice, E. A.; Kong, H. H.; Renaud, G.; Young, A. C.; NISC Comparative Sequencing Program; Bouffard, G. G.; Blakesley, R. W.; Wolfsberg, T. G.; Turner, M. L.; Segre, J. A. A Diversity Profile of the Human Skin Microbiota. *Genome Res.* **2008**, *18* (7), 1043–1050. https://doi.org/10.1101/gr.075549.107.

(7) Belkaid, Y.; Segre, J. A. Dialogue between Skin Microbiota and Immunity. *Science* **2014**, *346* (6212), 954–959. https://doi.org/10.1126/science.1260144.

(8) Chen, Y. E.; Fischbach, M. A.; Belkaid, Y. Skin Microbiota–Host Interactions. *Nature* **2018**, *553* (7689), 427–436. https://doi.org/10.1038/nature25177.

(9) Lai, Y.; Nardo, A. D.; Nakatsuji, T.; Leichtle, A.; Yang, Y.; Cogen, A. L.; Wu, Z.-R.; Hooper, L. V.; Schmidt, R. R.; Aulock, S. von; et al. Commensal Bacteria Regulate Toll-like Receptor 3–Dependent Inflammation after Skin Injury. *Nat. Med.* **2009**, *15* (12), 1377–1382. https://doi.org/10.1038/nm.2062.

(10) O'Neill, A. M.; Gallo, R. L. Host-Microbiome Interactions and Recent Progress into Understanding the Biology of Acne Vulgaris. *Microbiome* **2018**, *6* (1), 177. https://doi.org/10.1186/s40168-018-0558-5.

(11) Sanford, J. A.; Zhang, L.-J.; Williams, M. R.; Gangoiti, J. A.; Huang, C.-M.; Gallo, R. L. Inhibition of HDAC8 and HDAC9 by Microbial Short-Chain Fatty Acids Breaks Immune Tolerance of the Epidermis to TLR Ligands. *Sci. Immunol.* **2016**, *1* (4). https://doi.org/10.1126/sciimmunol.aah4609.

(12) Wanke, I.; Steffen, H.; Christ, C.; Krismer, B.; Götz, F.; Peschel, A.; Schaller, M.; Schittek, B. Skin Commensals Amplify the Innate Immune Response to Pathogens by Activation of Distinct Signaling Pathways. *J. Invest. Dermatol.* **2011**, *131* (2), 382–390. https://doi.org/10.1038/jid.2010.328.

(13) Ridaura, V. K.; Bouladoux, N.; Claesen, J.; Chen, Y. E.; Byrd, A. L.; Constantinides, M. G.; Merrill, E. D.; Tamoutounour, S.; Fischbach, M. A.; Belkaid, Y. Contextual Control of Skin Immunity and Inflammation by Corynebacterium. *J. Exp. Med.* **2018**, *215* (3), 785–799. https://doi.org/10.1084/jem.20171079.

(14) Chang, H.-W.; Yan, D.; Singh, R.; Liu, J.; Lu, X.; Ucmak, D.; Lee, K.; Afifi, L.; Fadrosh, D.; Leech, J.; et al. Alteration of the Cutaneous Microbiome in Psoriasis and Potential Role in Th17 Polarization. *Microbiome* **2018**, *6* (1), 154. https://doi.org/10.1186/s40168-018-0533-1.

(15) Gao, Z.; Tseng, C.; Strober, B. E.; Pei, Z.; Blaser, M. J. Substantial Alterations of the Cutaneous Bacterial Biota in Psoriatic Lesions. *PLoS ONE* **2008**, *3* (7). https://doi.org/10.1371/journal.pone.0002719.

(16) Stehlikova, Z.; Kostovcik, M.; Kostovcikova, K.; Kverka, M.; Juzlova, K.; Rob, F.; Hercogova, J.; Bohac, P.; Pinto, Y.; Uzan, A.; et al. Dysbiosis of Skin Microbiota in Psoriatic Patients: Co-Occurrence of Fungal and Bacterial Communities. *Front. Microbiol.* **2019**, *10*. https://doi.org/10.3389/fmicb.2019.00438.

(17) Kong, H. H.; Oh, J.; Deming, C.; Conlan, S.; Grice, E. A.; Beatson, M. A.; Nomicos, E.; Polley, E. C.; Komarow, H. D.; Program, N. C. S.; et al. Temporal Shifts in the Skin Microbiome Associated with Disease Flares and Treatment in Children with Atopic Dermatitis. *Genome Res.* **2012**, *22* (5), 850–859. https://doi.org/10.1101/gr.131029.111.

(18) Dekio, I.; Sakamoto, M.; Hayashi, H.; Amagai, M.; Suematsu, M.; Benno, Y. Characterization of Skin Microbiota in Patients with Atopic Dermatitis and in Normal Subjects Using 16S RRNA Gene-Based

Comprehensive Analysis. *J. Med. Microbiol.* **2007**, *56* (12), 1675–1683. https://doi.org/10.1099/jmm.0.47268-0.

(19) Paller, A. S.; Kong, H. H.; Seed, P.; Naik, S.; Scharschmidt, T. C.; Gallo, R. L.; Luger, T.; Irvine, A. D. The Microbiome in Patients with Atopic Dermatitis. *J. Allergy Clin. Immunol.* **2019**, *143* (1), 26–35. https://doi.org/10.1016/j.jaci.2018.11.015.

(20) Rosenthal, M.; Goldberg, D.; Aiello, A.; Larson, E.; Foxman, B. Skin Microbiota: Microbial Community Structure and Its Potential Association with Health and Disease. *Infect. Genet. Evol.* **2011**, *11* (5), 839–848. https://doi.org/10.1016/j.meegid.2011.03.022.

(21) Zeeuwen, P. L. J. M.; Kleerebezem, M.; Timmerman, H. M.; Schalkwijk, J. Microbiome and Skin Diseases. *Curr. Opin. Allergy Clin. Immunol.* **2013**, *13* (5), 514–520. https://doi.org/10.1097/ACI.0b013e328364ebeb.

(22) Hooper, L. V.; Wong, M. H.; Thelin, A.; Hansson, L.; Falk, P. G.; Gordon, J. I. Molecular Analysis of Commensal Host-Microbial Relationships in the Intestine. *Science* **2001**, *291* (5505), 881–884. https://doi.org/10.1126/science.291.5505.881.

(23) Turnbaugh, P. J.; Ley, R. E.; Mahowald, M. A.; Magrini, V.; Mardis, E. R.; Gordon, J. I. An Obesity-Associated Gut Microbiome with Increased Capacity for Energy Harvest. *Nature* **2006**, *444* (7122), 1027–1031. https://doi.org/10.1038/nature05414.

(24) Bäckhed, F.; Ding, H.; Wang, T.; Hooper, L. V.; Koh, G. Y.; Nagy, A.; Semenkovich, C. F.; Gordon, J. I. The Gut Microbiota as an Environmental Factor That Regulates Fat Storage. *Proc. Natl. Acad. Sci.* **2004**, *101* (44), 15718–15723. https://doi.org/10.1073/pnas.0407076101.

(25) Canesso, M. C. C.; Vieira, A. T.; Castro, T. B. R.; Schirmer, B. G. A.; Cisalpino, D.; Martins, F. S.; Rachid, M. A.; Nicoli, J. R.; Teixeira, M. M.; Barcelos, L. S. Skin Wound Healing Is Accelerated and Scarless in the Absence of Commensal Microbiota. *J. Immunol. Baltim. Md 1950* **2014**, *193* (10), 5171–5180. https://doi.org/10.4049/jimmunol.1400625.

(26) Meisel, J. S.; Sfyroera, G.; Bartow-McKenney, C.; Gimblet, C.; Bugayev, J.; Horwinski, J.; Kim, B.; Brestoff, J. R.; Tyldsley, A. S.; Zheng, Q.; et al. Commensal Microbiota Modulate Gene Expression in the Skin. *Microbiome* **2018**, *6*. https://doi.org/10.1186/s40168-018-0404-9.

(27) Ross, A. A.; Müller, K. M.; Weese, J. S.; Neufeld, J. D. Comprehensive Skin Microbiome Analysis Reveals the Uniqueness of Human Skin and Evidence for Phylosymbiosis within the Class Mammalia. *Proc. Natl. Acad. Sci.* **2018**, *115* (25), E5786–E5795. https://doi.org/10.1073/pnas.1801302115.

(28) Council, S. E.; Savage, A. M.; Urban, J. M.; Ehlers, M. E.; Skene, J. H. P.; Platt, M. L.; Dunn, R. R.; Horvath, J. E. Diversity and Evolution of the Primate Skin Microbiome. *Proc. R. Soc. B Biol. Sci.* **2016**, *283* (1822), 20152586. https://doi.org/10.1098/rspb.2015.2586.

(29) Corzo-León, D. E.; Munro, C. A.; MacCallum, D. M. An Ex Vivo Human Skin Model to Study Superficial Fungal Infections. *Front. Microbiol.* **2019**, *10*. https://doi.org/10.3389/fmicb.2019.01172.

(30) Rademacher, F.; Simanski, M.; Gläser, R.; Harder, J. Skin Microbiota and Human 3D Skin Models. *Exp. Dermatol.* **2018**, *27* (5), 489–494. https://doi.org/10.1111/exd.13517.

(31) Walter, S.; Rademacher, F.; Kobinger, N.; Simanski, M.; Gläser, R.; Harder, J. RNase 7 Participates in Cutaneous Innate Control of Corynebacterium Amycolatum. *Sci. Rep.* **2017**, *7* (1), 1–7. https://doi.org/10.1038/s41598-017-14383-z.

(32) Holland, D. B.; Bojar, R. A.; Jeremy, A. H. T.; Ingham, E.; Holland, K. T. Microbial Colonization of an in Vitro Model of a Tissue Engineered Human Skin Equivalent–a Novel Approach. *FEMS Microbiol. Lett.* **2008**, *279* (1), 110–115. https://doi.org/10.1111/j.1574-6968.2007.01021.x.

(33) Popov, L.; Kovalski, J.; Grandi, G.; Bagnoli, F.; Amieva, M. R. Three-Dimensional Human Skin Models to Understand Staphylococcus Aureus Skin Colonization and Infection. *Front. Immunol.* **2014**, *5*. https://doi.org/10.3389/fimmu.2014.00041.

(34) Timm, C. M.; Loomis, Kristin H; Stone, W.; Mehoke, Thomas; Brensinger, Bryan; Pellicore, M. R.; Staniczenko, Philip; Charles, Curtisha; Nayak, S.; Karig, David. Isolation and Characterization of Diverse Microbial Representatives from the Human Skin Microbiome. *Microbiome* **2020**.

(35) Pruesse, E.; Peplies, J.; Glöckner, F. O. SINA: Accurate High-Throughput Multiple Sequence Alignment of Ribosomal RNA Genes. *Bioinformatics* **2012**, *28* (14), 1823–1829. https://doi.org/10.1093/bioinformatics/bts252.

(36) Bolger, A. M.; Lohse, M.; Usadel, B. Trimmomatic: A Flexible Trimmer for Illumina Sequence Data. *Bioinformatics* **2014**, *30* (15), 2114–2120. https://doi.org/10.1093/bioinformatics/btu170.

(37) Patro, R.; Duggal, G.; Love, M. I.; Irizarry, R. A.; Kingsford, C. Salmon: Fast and Bias-Aware Quantification of Transcript Expression Using Dual-Phase Inference. *Nat. Methods* **2017**, *14* (4), 417–419. https://doi.org/10.1038/nmeth.4197.

(38) Soneson, C.; Love, M. I.; Robinson, M. D. Differential Analyses for RNA-Seq: Transcript-Level Estimates Improve Gene-Level Inferences. *F1000Research* **2015**, *4*, 1521. https://doi.org/10.12688/f1000research.7563.1.

(39) Love, M. I.; Huber, W.; Anders, S. Moderated Estimation of Fold Change and Dispersion for RNA-Seq Data with DESeq2. *Genome Biol.* **2014**, *15* (12), 550. https://doi.org/10.1186/s13059-014-0550-8.

(40) Pimentel, H.; Bray, N. L.; Puente, S.; Melsted, P.; Pachter, L. Differential Analysis of RNA-Seq Incorporating Quantification Uncertainty. *Nat. Methods* **2017**, *14* (7), 687–690. https://doi.org/10.1038/nmeth.4324.

(41) Supek, F.; Bošnjak, M.; Škunca, N.; Šmuc, T. REVIGO Summarizes and Visualizes Long Lists of Gene Ontology Terms. *PLOS ONE* **2011**, *6* (7), e21800. https://doi.org/10.1371/journal.pone.0021800.

(42) Micallef, L.; Rodgers, P. EulerAPE: Drawing Area-Proportional 3-Venn Diagrams Using Ellipses. *PLoS ONE* **2014**, *9* (7). https://doi.org/10.1371/journal.pone.0101717.

(43) Mi, H.; Muruganujan, A.; Huang, X.; Ebert, D.; Mills, C.; Guo, X.; Thomas, P. D. Protocol Update for Large-Scale Genome and Gene Function Analysis with the PANTHER Classification System (v.14.0). *Nat. Protoc.* **2019**, *14* (3), 703–721. https://doi.org/10.1038/s41596-019-0128-8.

(44) Ashburner, M.; Ball, C. A.; Blake, J. A.; Botstein, D.; Butler, H.; Cherry, J. M.; Davis, A. P.; Dolinski, K.; Dwight, S. S.; Eppig, J. T.; et al. Gene Ontology: Tool for the Unification of Biology. *Nat. Genet.* **2000**, *25* (1), 25–29. https://doi.org/10.1038/75556.

(45) Mi, H.; Muruganujan, A.; Ebert, D.; Huang, X.; Thomas, P. D. PANTHER Version 14: More Genomes, a New PANTHER GO-Slim and Improvements in Enrichment Analysis Tools. *Nucleic Acids Res.* **2019**, *47* (D1), D419–D426. https://doi.org/10.1093/nar/gky1038.

(46) Schneider, C. A.; Rasband, W. S.; Eliceiri, K. W. NIH Image to ImageJ: 25 Years of Image Analysis. *Nat. Methods* **2012**, *9* (7), 671–675.

Figures

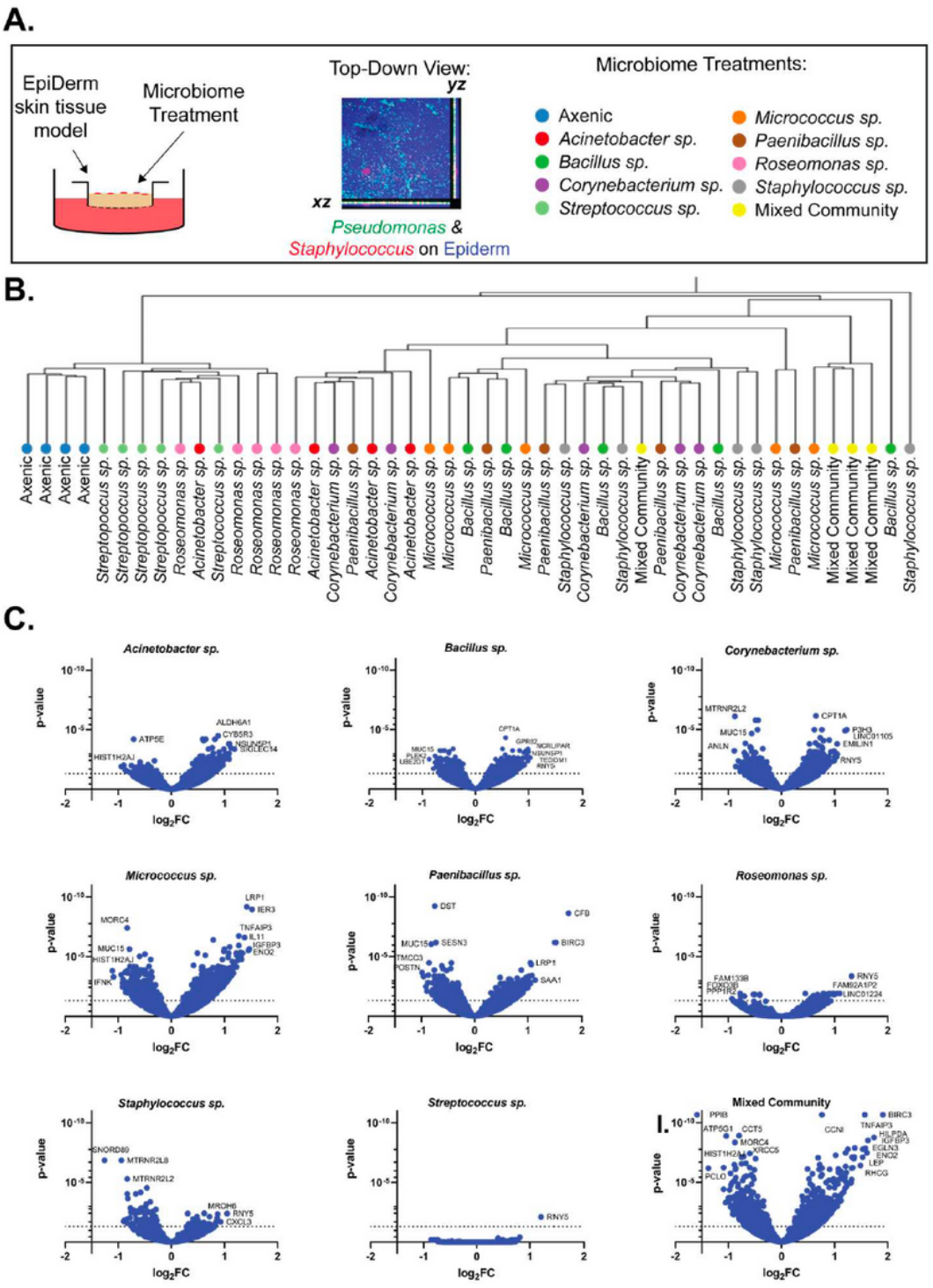


Figure 1

Global view of transcriptomics data (A) Experimental overview showing (left) a schematic of the 3D skin tissue culture system, (middle) a confocal image of EpiDerm skin tissue co-cultured with fluorescently labeled bacteria and (right) all microbiome treatments included in this study (B) Hierarchical clustering plot of replicate treatment conditions. (C) Volcano plots showing log2FC and adjusted p-values for genes of the indicated treatment condition compared to the axenic control.

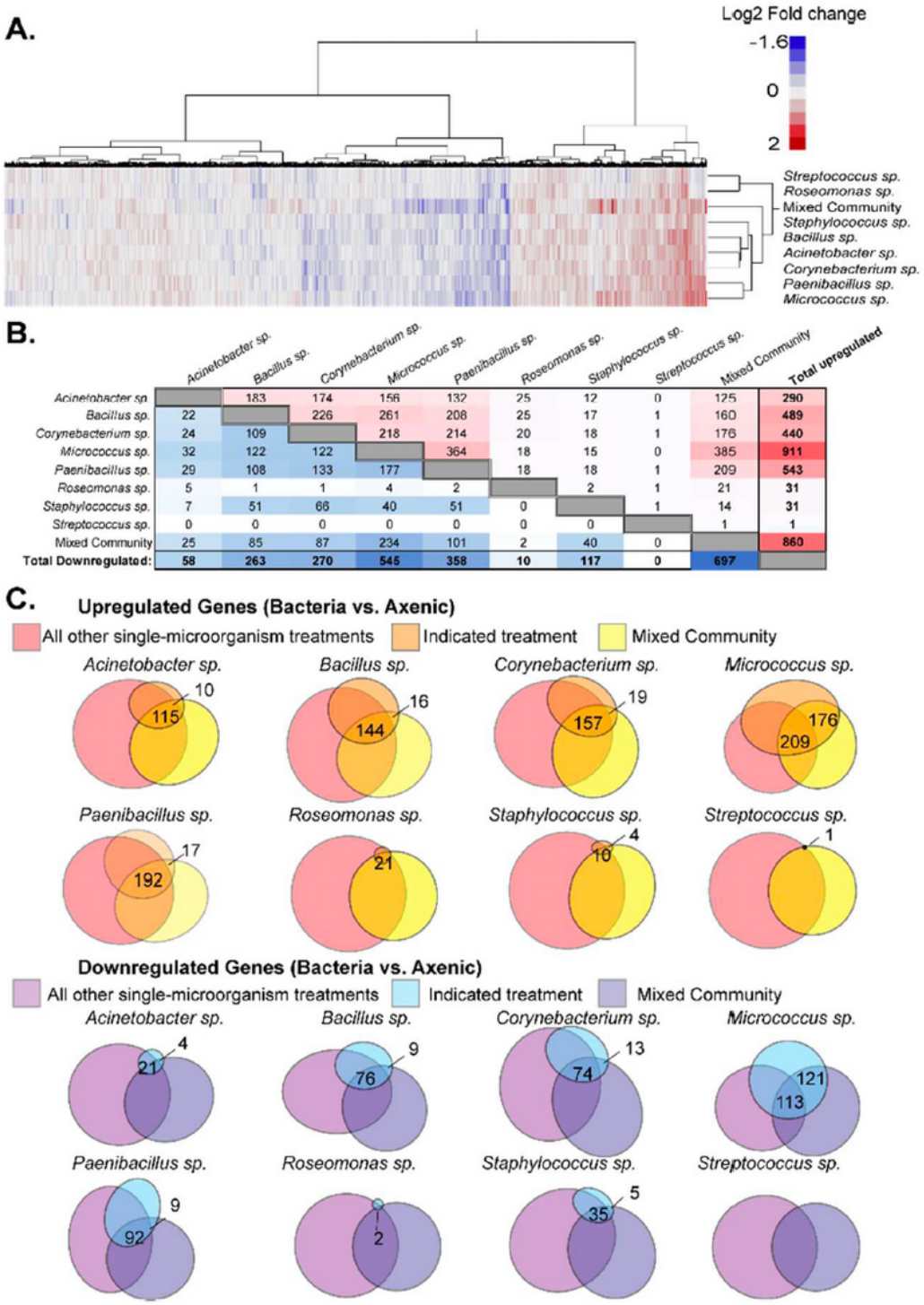


Figure 2

Comparison of differentially expressed genes across treatment groups (A) Heat map showing log2 fold change of gene expression for microbiome treatments groups compared to the axenic control. (B) The number of shared differentially expressed genes between treatment groups. Upregulated genes are on the top right of the plot and downregulated genes are shown on the bottom left. (C) Euler diagrams comparing the number of differentially expressed genes in the indicated treatment conditions to all other

single-microorganism treatments and the mixed community. Significantly altered gene expression was based on an adjusted p-value <0.05.

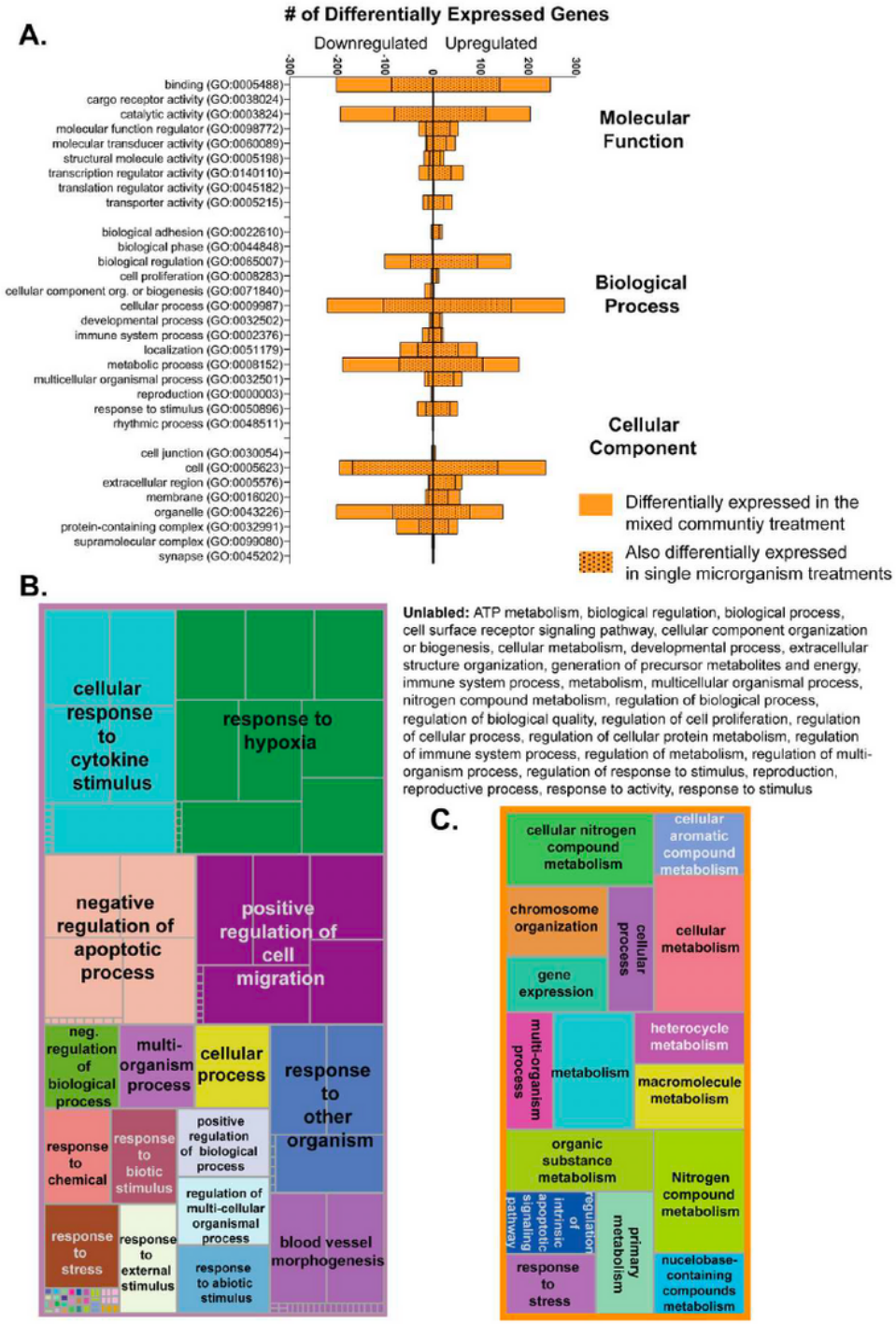


Figure 3

Gene sets overrepresented in mixed community treatment (A) PANTHER GO-Slim functional classification of differentially expressed genes in the mixed community and the single-microorganism treatment. (B) Treemap showing enriched biological process gene sets for genes differentially expressed between the

mixed community and axenic tissue. (C) Treemap showing enriched biological process gene sets for the genes which, compared to the axenic tissue, were differentially expressed in the mixed community but not differentially expressed in any single microorganism treatment. For treemaps, box size is indicative of enriched gene set significance. Genes with an adjusted p-value <0.05 were included in analyses.

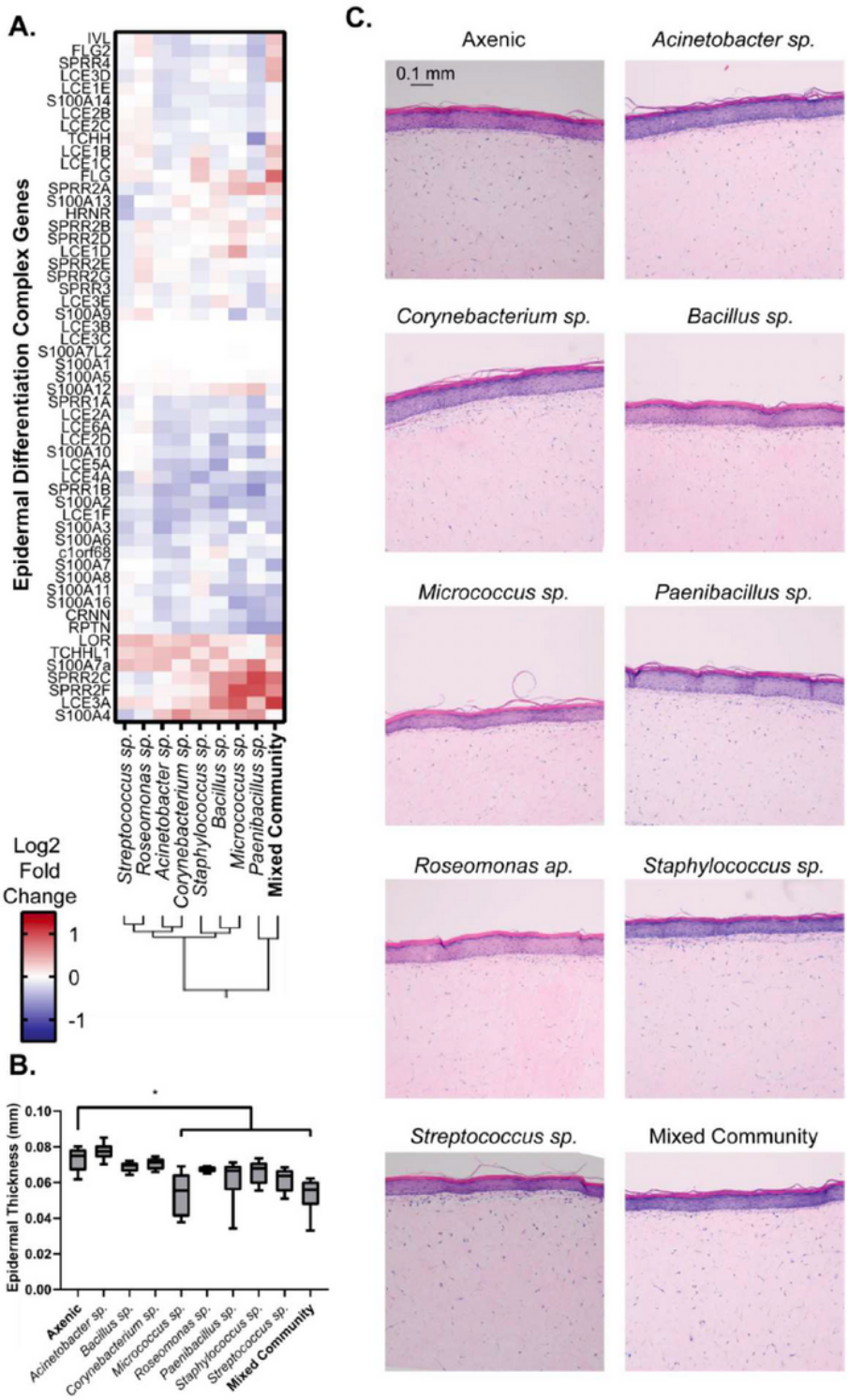


Figure 4

Microbiome treatments influence expression of epidermal differentiation genes (A) Heat map showing the expression of genes involved in the epidermal differentiation complex for each microbiome treatment. (B) Measurement of thickness of the nucleated epidermal region across five tissues. * indicates condition is different from the axenic control, Dunnett's test, $p<0.05$. (C) Representative H&E images of tissues with each treatment condition.

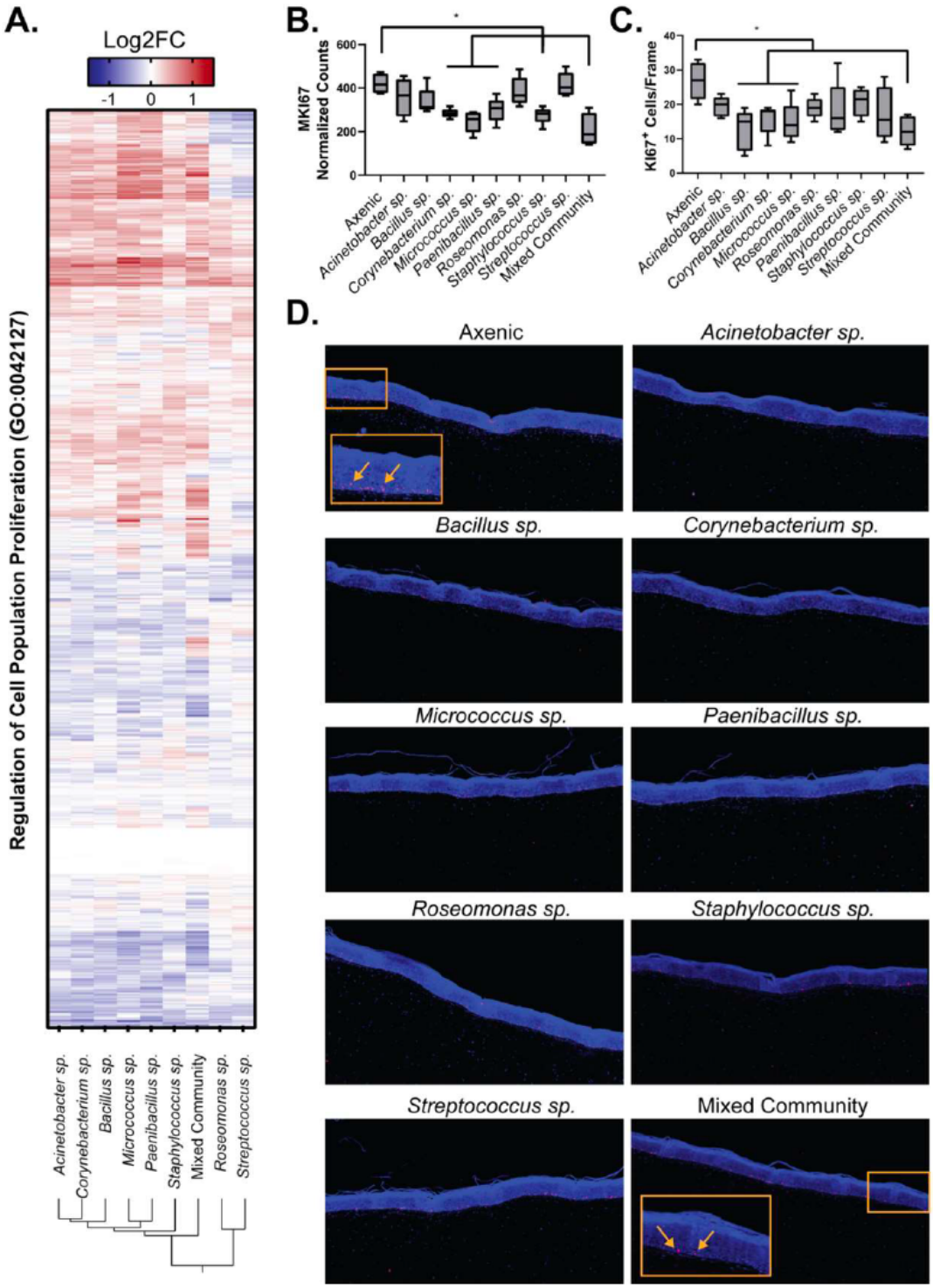


Figure 5

Microbiome treatment affects cell proliferation (A) Heat map showing the expression of genes in the ‘Regulation of cell proliferation’ gene set. (B) Normalized counts of the MIK67 in each treatment condition. (C) The number of KI67+ cells counted in each treatment condition, across four tissues. * indicates condition is different from the axenic control, one-way ANOVA followed by Dunnett’s multiple comparisons test against the axenic control, p<0.05 (D) representative immunofluorescence images of each treatment conditions showing DAPI-stained nuclei in blue and KI67 in red. Insets indicate a blowup of the indicated region.

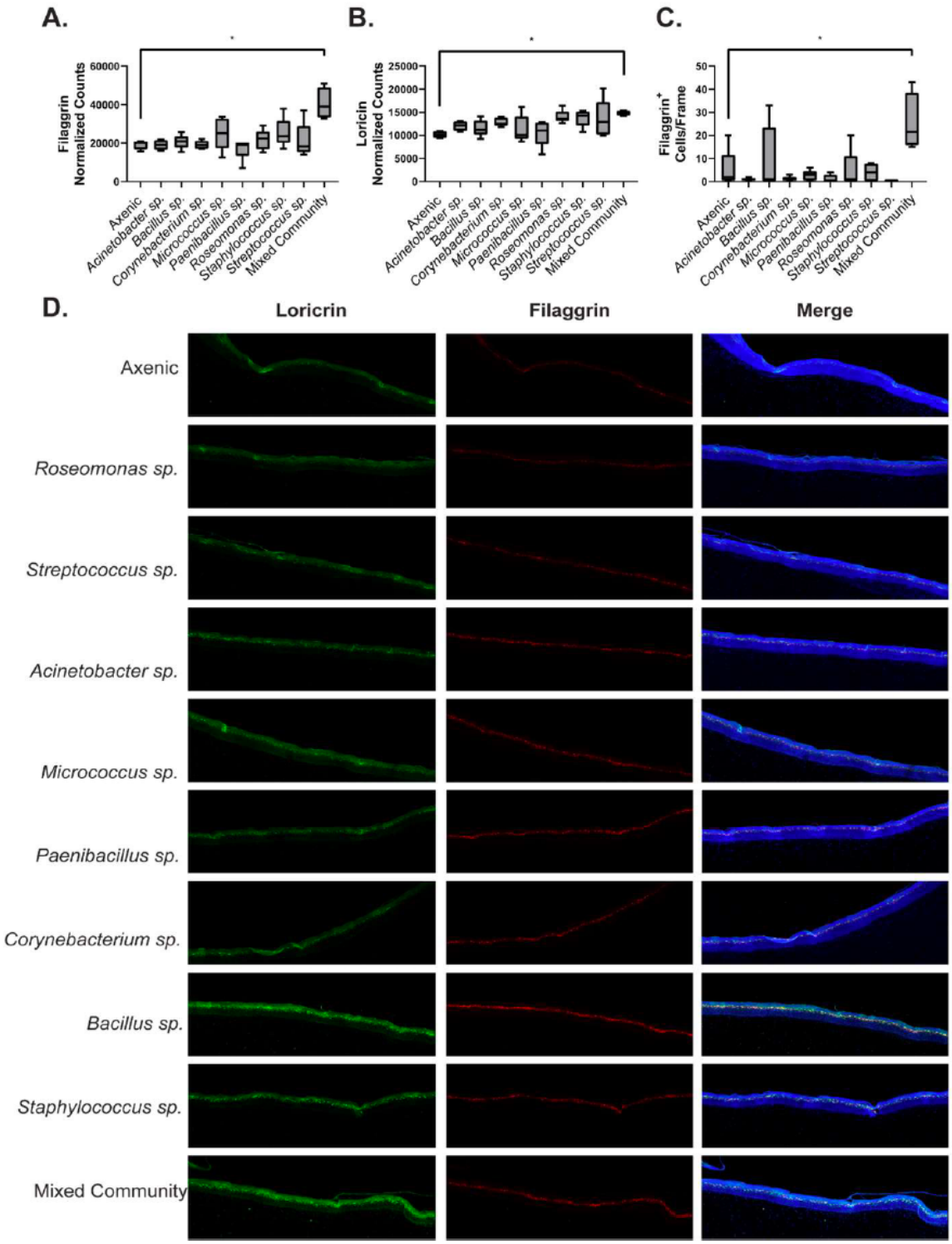


Figure 6

Microbiome treatment affects filaggrin and loricrin expression. Normalized counts of filaggrin (A) and loricrin (B) transcripts across treatment conditions. (C) The number of filaggrin+ cells counted in each treatment condition, across four tissues. * indicates condition is different from the axenic control, one-way ANOVA followed by Dunnett's multiple comparison's test against the axenic control, $p<0.05$

Supplementary Files

This is a list of supplementary files associated with this preprint. Click to download.

- 3.QualityAssessmentofRNASequencingData.xlsx
- 2.OpticalDensityandCFUStandardization.pdf
- 1.MicroorganismIsolateInformation.xlsx
- 5.GeneSetAnalysisData.xlsx
- 4.DifferentialGeneExpressionData.xlsx